KINETIC STUDY AND MECHANICAL QUALITATIVE CONTROL OF AISI 4140 BORONIZED STEEL FOCUSED ON THE ROLE OF THE AUSTENITIC TRANSFORMATION OF THE SUBSTRATE DURING THE PROCESS

Dimitrios I. Zagkliveris*, Olga Valentini I. Tyrilou, Georgios K. Triantafyllidis

Dept. of Chemical Engineering, Aristotle University of Thessaloniki, A.U.Th. Campus, Thessaloniki 54124, Greece

Abstract

In this study a series of boronizing experiments was performed on AISI 4140 steel's surface in temperature and time ranges 1073 – 1273 K and 4 – 12 hours, respectively. The well known pack boronizing method was applied and a thick dense, verified with XRD characterization, Fe_2B layer was formed, with thickness reaching 160 μm. The material showed a satisfactory response to the boronizing treatment, except for the long-lasting experiments (12 hours), in which the coating was significantly thinner in comparison to the theoretical expectation, due to adsorbed boron depletion. After applying a Fick's Law-based model and extracting the kinetic parameters, we observed an alteration of the diffusion coefficient of boriding related to austenitizing crystallographic transformation of the ferrous substrate. Additionally, enhancing the results of the kinetic study, an evaluation of the quality of the boride coating was operated via micro-Vickers and Rockwell C (VDI 3198) indentation tests, complemented with optical and SEM imaging. Vickers measurements varied between 1500 HV and 2200 HV. Rockwell C qualification test results were excellent at specific boronizing conditions, proving that boronizing is one of the most advantageous superficially protective techniques for steels.

Keywords: *coating technology, diffusion, kinetics, mechanical properties, scanning electron microscopy, X-ray diffraction, boriding, steels*

1. INTRODUCTION

AISI 4140 steel is a general purpose high tensile steel with chromium and molybdenum as main alloying elements. It is often provided in a quenched and tempered condition, in which the material represents excellent toughness, ductility and wear resistance [1]. However, its chromium composition is low and cannot enhance its corrosion resistance. Moreover, the most common uses of AISI 4140 cover many industrial fields and include machinery parts, shafts, gears etc [1].

A superficial protection of the material against wear and corrosion could upgrade its properties and widen the range of its applications, prolonging significantly the lifetime of the components. The most efficient surface protecting method for ferrous alloys is the boronizing process. It is referred that it can multiply the life time of a component by a factor 3 to 10 [2].

Boronizing (or boriding) is a temperature activated thermochemical treatment, in which boron atoms are being diffused into the substrate metal lattice pushed by chemical potential gradient between substrate and its environment and supported by externally provided heat energy [3]. A number of special techniques for boronizing have been developed in the last 60 years, such as simple pack or paste, electrochemical, plasma, microwave assisted, gas, laser boriding and other methods [4], [5], [6], [7].

During boronizing of ferrous alloys, e.g. steels, two types of metal borides it is possible to be formed: FeB and Fe_2B. FeB is a boron-rich boride that appears when the concentration of diffused boron exceeds 50% mol. However, its formation and growth rate depends also on the present alloying elements of the substrate [8]. This boride is a very hard, but also brittle compound [3]. Thus, its formation is sometimes undesirable. Fe_2B is being formed anyway and is the main or even the only constituent of the coating layer. It displays reduced brittleness, in comparison with FeB [3], and provides excellent superficial protection against wear and corrosion phenomena [9].

In the literature, there are a number of studies on AISI 4140's behavior in boronizing [9], [10], [11], [12], [13], [14]. However, none of them is carried out at a wide temperature range, including conditions before and after the austenitizing temperature, equally.

In our study, we attempt to investigate the kinetics of boriding the AISI 4140 steel and to evaluate the durability of the coating against mechanical load application via micro-Vickers measurements and a special Rockwell-C indentation test (VDI 3198) [15] and to estimate the influence of the boriding temperature to the mechanical strength of the boride layer [16]. We also aim to highlight the effect of the α→γ crystallographic transformation of the substrate to the kinetics of boriding, by affecting the values of diffusion coefficient.

2. THEORETICAL MODEL OF DIFFUSION

2.1. Fick's Second Law

The boriding process is a diffusion dominated phenomenon, which occurs in non steady-state conditions. Thus, the most appropriate way to describe it mathematically is by using Fick's Second Law of Diffusion.

The symbols and letters used in the following modeling procedure are based on graphic description of diffusion presented in **Fig. 1**.

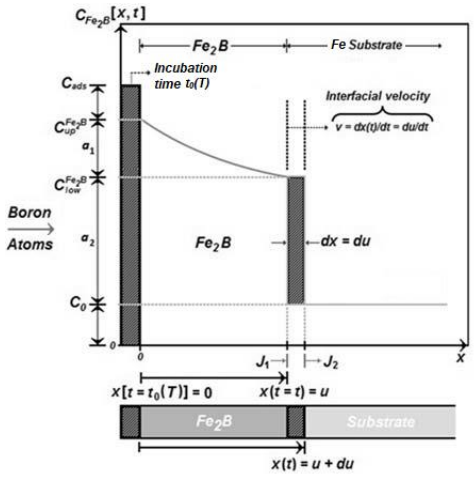


Fig. 1: Boron concentration profile in the boride layer during boronizing process

In order to apply this model in our system, it is necessary to set the following assumptions:

i. The substrate is a semi-infinite medium, in which the concentration of diffused boron depends only on the position x in the medium and the time t.

ii. Boron diffusion through the simultaneously being formed Fe_2B phase is the unique moving mechanism of boron in the system.

iii. Boron diffusion occurs only perpendicularly to the specimen's surface, creating a linear Fe_2B-substrate interface.

iv. The influence of the alloying elements is not considered.

v. There is an incubation time, which refers to the time needed for the nucleation of Fe_2B superficially and depends on the boriding temperature, $t_0(T)$.

vi. Any volume change during phase transformations is not considered.

vii. The whole system is in thermal equilibrium, thus all regions have the same temperature during the treatment.

Taking into consideration of the aforementioned assumptions, we establish the differential equation of Fick's Law as follows:

$$\frac{\partial C(x(t),t)}{\partial t} = D_{\mathrm{Fe_2B}} \frac{\partial^2 C(x(t),t)}{\partial x^2} \quad \text{(Eq. 1)}$$

The general solution of **Eq. 1** is the following:

$$C(x(t),t) = A + B \cdot \mathrm{erf}\left(\frac{x(t)}{\sqrt{4D_{\mathrm{Fe_2B}}t}}\right) \quad \text{(Eq. 2)}$$

where *A* and *B* are constants, which can be defined by the following initial and boundary conditions:

- $C(x,0) = 0$ (there is no boron in the substrate before treatment)
- $C\big(0, t_0(T)\big) = C^{\mathrm{up}}_{Fe_2B}$ (at the end of the incubation period, boron concentration in Fe_2B superficially gets its maximum value)
- $C(u,t) = C^{\mathrm{low}}_{\mathrm{Fe_2B}}$ (at the Fe_2B/Fe interface ($x = u$), boron maintains a constant minimum concentration during the experiment)

By applying these conditions in **Eq. 2**, we determine the constants A and B:

$$A = C^{\mathrm{up}}_{\mathrm{Fe_2B}} \quad \& \quad B = \frac{C^{\mathrm{low}}_{\mathrm{Fe_2B}} - C^{\mathrm{up}}_{\mathrm{Fe_2B}}}{\mathrm{erf}\left(\frac{u}{\sqrt{4D_{\mathrm{Fe_2B}}t}}\right)} \quad \text{(Eq. 3)}$$

Additionally, according to the parabolic growth law, $u = k_{\mathrm{Fe_2B}}\sqrt{t - t_0(T)}$, where $k_{\mathrm{Fe_2B}}$ is the parabolic law constant. Consequently, after importing parabolic law into **Eq. 3** and combining **Eq. 3** with **Eq. 2**, we conclude to the final boron concentration profile equation:

$$C(x(t),t) = C^{\mathrm{up}}_{\mathrm{Fe_2B}} + \frac{C^{\mathrm{low}}_{\mathrm{Fe_2B}} - C^{\mathrm{up}}_{\mathrm{Fe_2B}}}{\mathrm{erf}\left(\frac{k_{\mathrm{Fe_2B}}\left[1-\frac{t_0(T)}{t}\right]^{1/2}}{\sqrt{4D_{\mathrm{Fe_2B}}}}\right)} \cdot \mathrm{erf}\left(\frac{x(t)}{\sqrt{4D_{\mathrm{Fe_2B}}t}}\right) \quad \text{(Eq. 4)}$$

2.2. Mass balance equation

In order to eliminate the variable $C(x(t),t)$, it is necessary to establish the mass balance equation at the Fe_2B/Fe interface:

$$C^{\mathrm{low}}_{\mathrm{Fe_2B}} \cdot \left(\frac{dx(t)}{dt}\right)\Big|_{x=u} = -D_{\mathrm{Fe_2B}} \cdot \left(\frac{\partial C(x(t),t)}{\partial x(t)}\right)\Big|_{x=u} \quad \text{(Eq. 5)}$$

2.3. Final equation – Calculation of D_{Fe_2B}

By substituting $C(x(t),t)$ from **Eq. 4** in **Eq. 5** we get:

$$C^{\mathrm{low}}_{\mathrm{Fe_2B}} \cdot \left(\frac{dx(t)}{dt}\right)\Big|_{x=u} = -D_{\mathrm{Fe_2B}} \cdot \frac{C^{\mathrm{low}}_{\mathrm{Fe_2B}} - C^{\mathrm{up}}_{\mathrm{Fe_2B}}}{\mathrm{erf}\left(\frac{k_{\mathrm{Fe_2B}}\left[1-\frac{t_0(T)}{t}\right]^{1/2}}{\sqrt{4D_{\mathrm{Fe_2B}}}}\right)} \cdot \frac{\partial}{\partial x(t)} \mathrm{erf}\left(\frac{x(t)}{\sqrt{4D_{\mathrm{Fe_2B}}t}}\right)\Big|_{x=u} \quad \text{(Eq. 6)}$$

After the execution of the calculations we conclude to the final equation:

$$C_{Fe_2B}^{low} \cdot k_{Fe_2B} = -2\sqrt{\frac{D_{Fe_2B}}{\pi}} \cdot \frac{C_{Fe_2B}^{low} - C_{Fe_2B}^{up}}{\operatorname{erf}\left(\frac{k_{Fe_2B}\left[1-\frac{t_0(T)}{t}\right]^{1/2}}{\sqrt{4D_{Fe_2B}}}\right)} \cdot \exp\left(-\frac{k_{Fe_2B}^2\left[1-\frac{t_0(T)}{t}\right]}{4D_{Fe_2B}}\right) \quad \text{(Eq. 7)}$$

The parabolic law constant can be extracted from the experimental data. Thus, we import the experimental values of k_{Fe_2B} into **Eq. 7** and, applying a numerical approximation method, we can calculate the diffusion coefficient D_{Fe_2B}. It is significant to emphasize that the relationship between k_{Fe_2B} and D_{Fe_2B} is time-dependent. Thus, the calculation must be carried out for each exposure time of boriding, separately.

Additionally, diffusion coefficient is temperature activated and follows a typical Arrhenius behavior:

$$D_{Fe_2B}(T) = D_0 e^{-Q/RT} \quad \text{(Eq. 8)}$$

where D_0 is a pre-exponential constant and Q is the activation energy of boron atoms regarding its transition to the next interstitial vacancy in the substrate crystal lattice during diffusion. Q is a thermodynamic quantity and can be theoretically estimated by using appropriate thermodynamic models [17].

3. MATERIALS AND METHODS

The AISI 4140 raw material was provided in Φ20 mm cylindrical rods. We cut 1 cm thick slices, which have been divided into quarters. The samples were grinded and polished. Each specimen was placed in a crucible fulfilled with the boronizing powder, consisted of 80% SiC as filler, 10% B_4C as boron source and 10% KBF_4 as reaction activator. Afterwards, the thermochemical process of boriding took place in a conventional CARBOLITE SWF 1300 furnace in conditions, which vary between 1073 K and 1273 K temperature with 50 K step and between 4 hrs and 12 hrs time with 2 hrs step (totally 25 successful experiments).

After boriding, the coated specimens were cleaned from remaining powder grains and undergo XRD measurements by a BRUKER D8 Advance X-Ray diffractometer, in order to verify the formation of the desirable borides.

Subsequently, the VDI 3198 test was carried out. The diamond conical indenter of Rockwell-C scale was used and a load of 1471 N was applied. The machine used is an INNOVATEST 600MA model. The indentations were made on the borided surface, in order to evaluate its endurance against point load application. The specifications of the method are presented in **Fig. 2** [15]. For the test were selected all the specimens that had been borided for 8 hrs. Thus, a conclusion related to the influence of the boriding temperature in the durability of the coating would be extracted. The indentations were studied using Scanning Electron Microscopy.

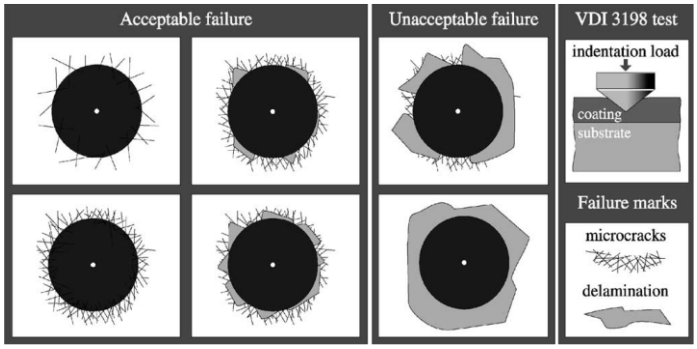


Fig. 2: The principle of the VDI 3198 indentation test. Source: [15]

Finally, a metallographic analysis was performed, in order to determine the thickness of the boride layer for further study on the kinetic parameters of the process. The captures were taken by an OLYMPUS DP50 camera mounted on an OLYMPUS AX70 optical microscope. The images were analyzed using Image-Pro Plus software tools.

Complementarily to the VDI 3198 mechanical strength test, a micro-Vickers hardness profile across the coating layer was constructed, using an AFFRI DM2 device.

4. RESULTS AND DISCUSSION

4.1. The VDI 3198 indentation test

First, the results of the VDI 3198 test are presented. In **Figs. 3-7** the indentations on the coated surface of the specimens that had been boronized for 8 h are depicted. The edge of the created indentation is approximately indicated with a gray circle, where needed. The most visible cracks are indicated by a yellow asterisk "*".

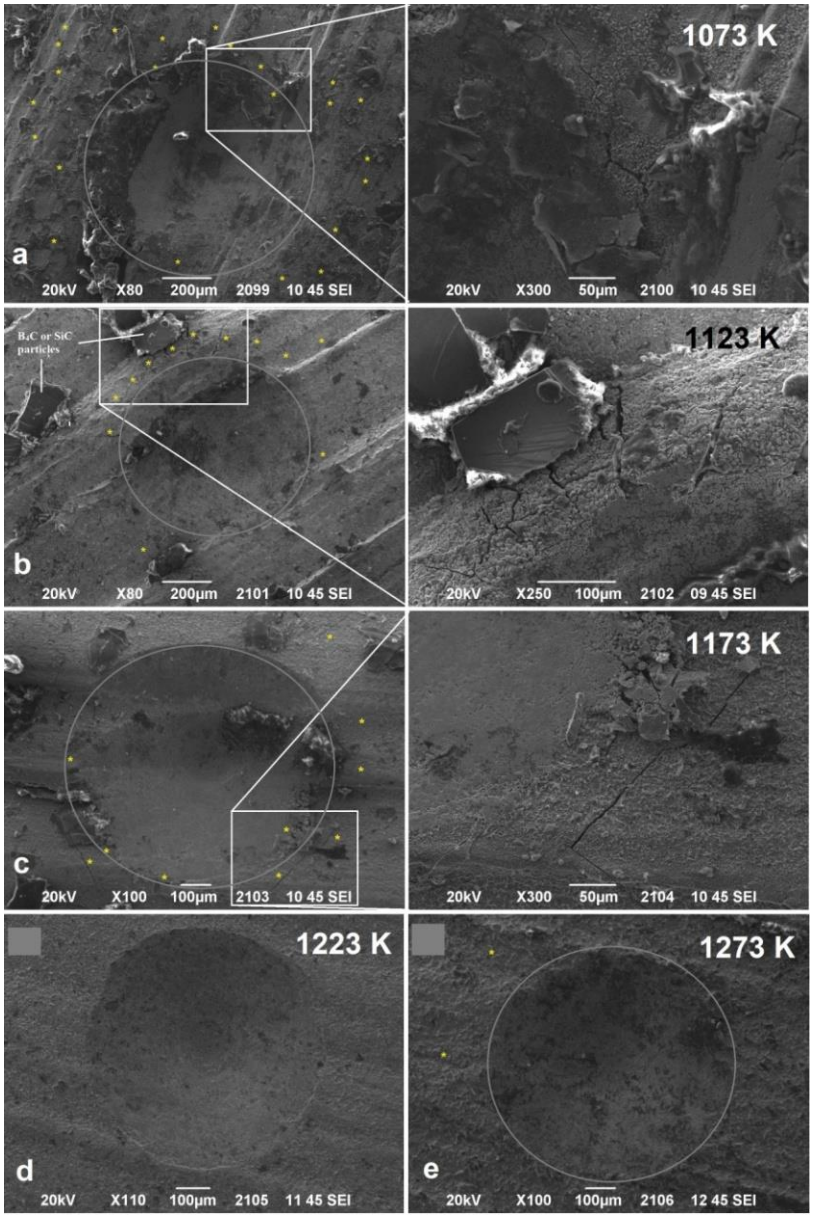


Fig. 3: SEM image of indentation on the specimen boronized at a) 1073 K, b) 1123 K, c) 1173 K, d) 1223 K and e) 1273 K

The number of cracks is clearly reduced as the boronizing temperature rises.

In particular, at 1073 K (**Fig. 3a**) and 1123 K (**Fig. 3b**), many cracks were detected. In addition, the distance between them is such that they often cross each other to create extended networks.

At 1173 K (**Fig. 3c**), the cracks are significantly fewer, and no networks were detected. Nevertheless, the total number is still considerable.

At higher temperatures (**Fig. 3d-e**), we observe excellent conditions, with the total absence of any type of failure.

In any case, even at the lowest temperature, no delamination was detected, and the results of the test were considered acceptable, according to **Fig. 2**. Moreover, our results in this study reflect the superior durability of the boride coating compared with the results of similar studies in the literature [18], [19], [20].

The thickness of the coating and the absence of the brittle FeB phase are undoubtedly the main factors leading to its durability against point loads, but the abrupt improvement at 1223 K (**Fig. 3d**) requires further explanation. Remarkably, this temperature is slightly higher than the austenitizing temperature of the substrate, which leads us to conclude that stronger coatings are produced by boronizing on an austenite substrate crystal structure. Subsequently, this possible conclusion will be correlated with the results of the application of the theoretical model to thickness measurements obtained from a metallographic analysis.

4.2. Micro-Vickers hardness characterization

In **Fig. 4**, the micro-Vickers hardness profile is presented.

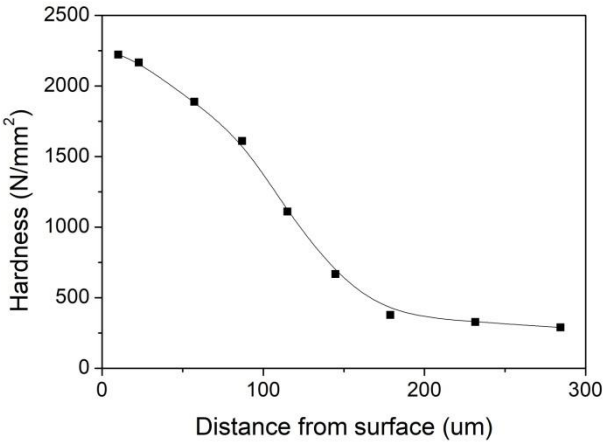


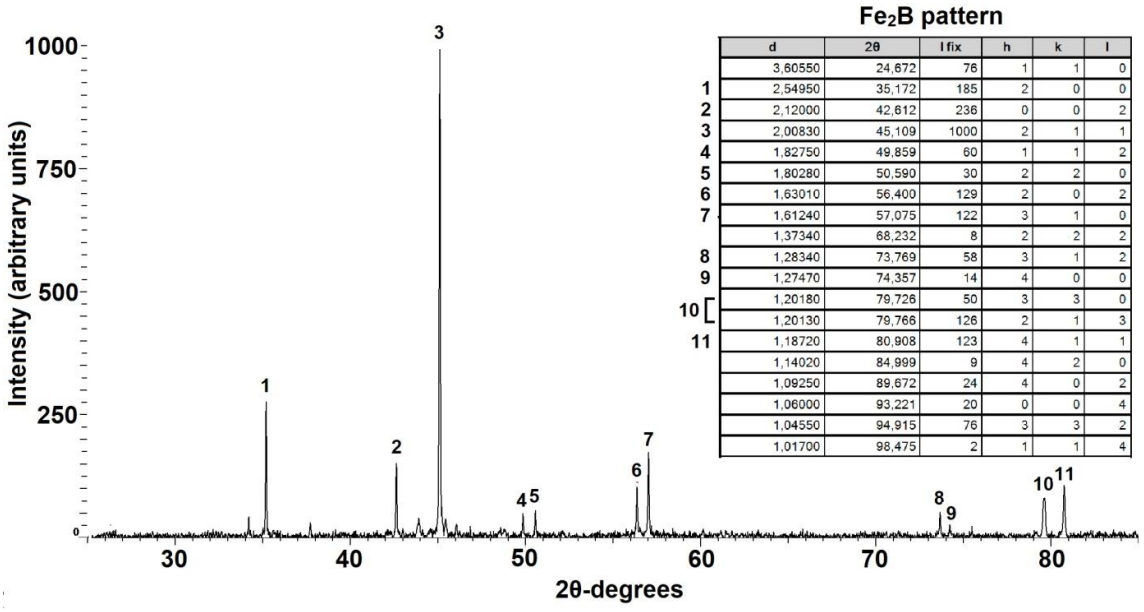
Fig. 4: Micro-Vickers hardness profile of the boride layer

As shown in **Fig. 4**, the hardness of the boride layer starts at approximately 2250 N/mm^2 close to the surface and decreases gradually until stabilizing at approximately 280 N/mm^2, which is the average hardness of the perlitic substrate. There are two main reasons for this gradual decrease: a) Close to the surface, the concentration of boron in the Fe_2B phase is at its maximum, but it decreases gradually towards the substrate. The hardness of the Fe_2B phase rises with the boron concentration via a solid solution strengthening mechanism [21], [22], [23]. b) In the inner sublayer ($x \geq \sim 100$ μm) a tooth-like morphology is dominant. Thus, the Vickers indenter cannot cover a clear Fe_2B area, because of the relatively small width of the "teeth". Therefore, this sublayer displays a decreased hardness compared to that of the pure Fe_2B phase.

Regardless of the reason, a gradual decrease in the hardness towards the substrate is desirable as an abrupt and intense decrease in the hardness would be destructive during mechanical stress applications.

4.3. Crystallographic characterization of the boride layer via XRD

The XRD spectrum of the surface of the coating layer is presented in **Fig. 8**. The pattern reveals that the coating consists exclusively of the Fe_2B phase. In the table inside the figure, the crystallographic data of the Fe_2B phase from the Crystallographic Open Database are depicted to confirm our conclusion.



	d	2θ	I fix	h	k	l
	3,60550	24,672	76	1	1	0
1	2,54950	35,172	185	2	0	0
2	2,12000	42,612	236	0	0	2
3	2,00830	45,109	1000	2	1	1
4	1,82750	49,859	60	1	1	2
5	1,80280	50,590	30	2	2	0
6	1,63010	56,400	129	2	0	2
7	1,61240	57,075	122	3	1	0
	1,37340	68,232	8	2	2	2
8	1,28340	73,769	58	3	1	2
9	1,27470	74,357	14	4	0	0
10	1,20180	79,726	50	3	3	0
	1,20130	79,766	126	2	1	3
11	1,18720	80,908	123	4	1	1
	1,14020	84,999	9	4	2	0
	1,09250	89,672	24	4	0	2
	1,06000	93,221	20	0	0	4
	1,04550	94,915	76	3	3	2
	1,01700	98,475	2	1	1	4

Fig. 5: XRD spectrum of the surface of the boride coating

The relative intensity of all of the peaks is in agreement with the literature values ("I fix" column in the table of **Fig. 5**), which means that no preferred growth orientation of the Fe_2B crystals is detected. Generally, during boronization, the tooth-like crystals prefer to grow along the [001] crystallographic orientation [24]. However, when the coating is quite thick, the crystals in the upper layers often display a weak or totally absent anisotropy [24]. In our measurement, a Cu Ka X-ray beam (λ = 1.5406 Å) was used. According to [25], the X-ray penetration depth in Fe at this wavelength is approximately 36 μm (in this case, the Fe_2B phase can safely be considered to be like pure Fe). Thus, the X-ray penetration is shallow compared to the total thickness of the coating (more than 100 μm). Consequently, only the isotropic upper layers of the boride coating contribute to the diffraction. As a result, we obtained the nontextured spectrum of **Fig. 5**.

4.4. Application of the experimental data to the theoretical model of the diffusion kinetics

The experimental values of the mean coating thickness of all specimens are presented in **Table I**.

Table I: Average thickness values of the Fe_2B coating layers for various boronizing conditions

Temperature (K)	**1073**	**1123**	**1173**	**1223**	**1273**
Time (h)	**Average Fe_2B layer thickness and standard deviation (μm)**				
4	27.7±1.9	45.2±3.9	65.2±2.5	80.7±6.4	101.0±8.0
6	43.7±2.3	57.6±2.7	94.7±5.5	119.8±7.7	132.2±9.2
8	52.9±2.2	73.8±5.1	117.3±4.0	135.1±11.3	150.2±5.8
10	60.1±3.3	84.4±5.1	126.0±8.1	142.1±8.4	163.8±10.6
12	46.8±1.7	53.8±2.7	56.5±5.0	86.0±4.2	117.4±6.8

By inserting the data of **Table I** into a chart, we obtain the results shown in **Fig. 6**.

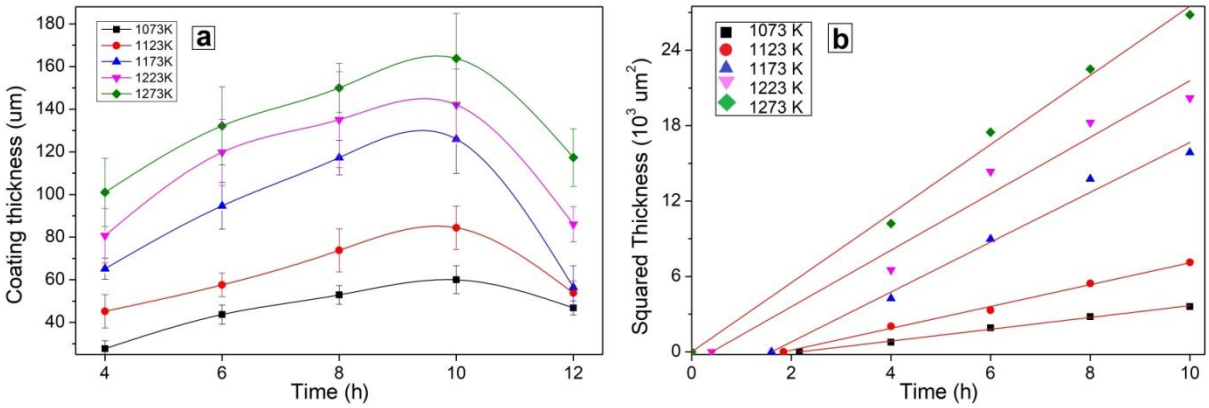


Fig. 6: (a): Coating thickness versus boriding time, (b): squared thickness versus boriding time

From **Fig. 6a**, one can easily observe that the coating thickness was significantly diminished after boronizing treatments that lasted for 12 h. This result was unexpected, considering that, according to the parabolic law, the coating thickness *x* varied proportionately to $t^{1/2}$; thus, $x(t)$ should be a strictly increasing function of time.

We attempted to explain the apparent decrease in the thickness by invoking the boron depletion phenomena. We believe that the key parameter is the concentration of adsorbed boron on the surface C_{ads} (depicted in **Fig. 1**). According to the adsorption kinetics, we can define the rate of boron adsorption as follows [26]:

$$-\frac{dC_{\text{ads}}}{dt} \equiv R_{\text{ads}} = \frac{f(\theta)\cdot P(t)}{\sqrt{2\pi mRT}}\cdot e^{-E_{\text{a}}(\theta)/RT} \qquad \text{(Eq. 9)}$$

where $f(\theta)$ is an undetermined function of the coverage fraction θ, $P(t)$ is the time-dependent partial pressure of boron just above the surface, m is the atomic weight of boron, *k* is the Boltzmann constant, $E_{\text{a}}(\theta)$ is the coverage-dependent activation energy of adsorption, and *T* is the absolute temperature.

Assuming that a mass equilibrium is established on the surface during the experiment, we can assume that the coverage fraction θ, remains constant over time. Moreover, the boron partial pressure follows an exponential behavior, $P(t) = ae^{-bt}$, with a and b constants. Consequently, by integrating **Eq. 9**, we obtain:

$$C_{\text{ads}}(t) = \int_0^t \frac{dC_{\text{ads}}}{dt}\,dt = -\frac{f(\theta)}{\sqrt{2\pi mRT}}\cdot e^{-E_{\text{a}}(\theta)/RT}\cdot\int_0^t ae^{-bt}\,dt$$

Finally,

$$C_{\text{ads}}(t) = \frac{af(\theta)}{b\sqrt{2\pi mRT}}\cdot e^{-E_{\text{a}}(\theta)/RT}\cdot e^{-bt} \qquad \text{(Eq. 10)}$$

In a concise form, we have an expression of C_{ads} as a function of time:

$$C_{\text{ads}}(t) = K\cdot e^{-bt} \qquad \text{(Eq. 11)}$$

where *K* is a constant value for a given temperature. C_{ads} decreases exponentially with time, thereby causing a depletion of boron on the surface. However, the a and b constants in **Eq. 10** may depend on the experimental parameters, e.g., the total amount of boron in the crucible and how efficiently it is sealed inside.

On the other hand, the boron diffusion undergoes a positive progress for as long as $C_{\text{ads}} \geq C^{\text{up}}_{\text{Fe}_2\text{B}}$. From the moment that C_{ads} becomes minor to $C^{\text{up}}_{\text{Fe}_2\text{B}}$, a reverse diffusion of boron begins to occur because of the inverted sign of its chemical potential. As a result, boron atoms move from the coating layer towards the surface clearing out the substrate and decreasing the thickness of the Fe_2B phase.

According to the experimental data in **Fig. 6a**, such a reverse diffusion process seems to occur for t > 10 h. Hence, to proceed to the kinetic study, it is necessary to exclude from our source data the experiments that were carried out at t = 12 h. Hereafter, it will be considered that: 4 h ≤ t ≤ 10 h. By plotting the squared thickness values versus the time for each temperature, **Fig. 6b** is produced.

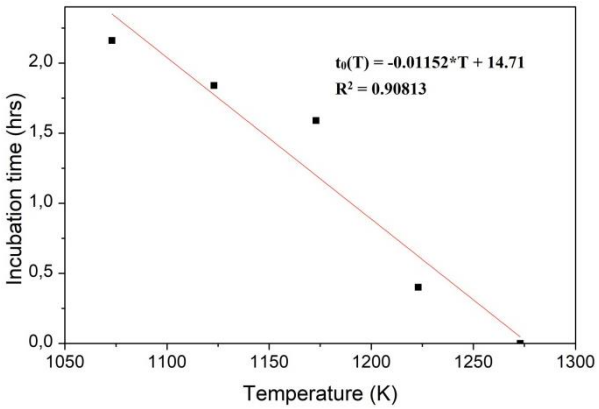


Fig. 7: Incubation time versus boriding temperature

The incubation time can be approximately determined by the following linear equation, which is graphically extracted by linear regression in **Fig. 7**:

$$t_0(T) = -0.01152 \cdot T + 14.71 \qquad \text{(Eq. 13)}$$

The R^2 value of the least squares regression (R^2 = 0.90813) reveals a roughly linear approximation. This is related to the fact that the t_0 values were estimated graphically from **Fig. 7**. Using this method, the precision of the evaluation of t_0 is very sensitive to all experimental and measurement errors that might have previously occurred.

From the slope of the regression lines in **Fig. 6b**, we extracted the parabolic constant $k_{\text{Fe}_2\text{B}}$ values for each temperature. Afterwards, applying the Newton-Raphson approximation method in **Eq. 7**, we obtaind the desired diffusion coefficient $D_{\text{Fe}_2\text{B}}$ values. We repeated this calculation for all of the experimental time values and the results are plotted in **Fig. 8**.

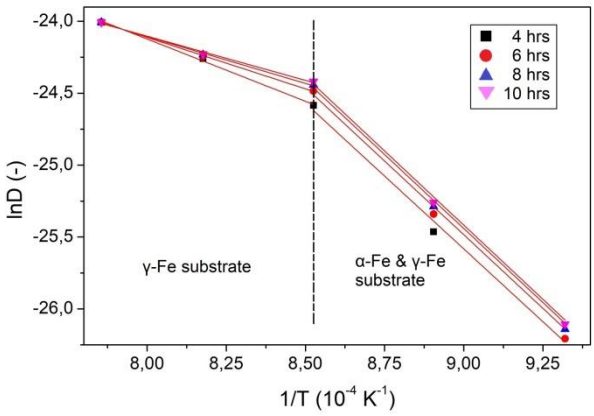


Fig. 8: Logarithmic diagram of diffusion coefficient $D_{\text{Fe}_2\text{B}}$ as a function of 1/T

In **Table II,** the temperature dependent expression $D_{Fe_2B}(T)$ for each experimental condition is presented.

Table II: Exponential expressions of $D_{Fe_2B}(T)$ for all experimental conditions

Boriding time (h)	**Diffusion coefficient D(T) (m^2/s)**	
	$T < 1173$ K	$T > 1173$ K
4	$6.466 \cdot 10^{-4} \cdot \exp(-20{,}265.3/T)$	$3.403 \cdot 10^{-8} \cdot \exp(-8{,}658.8/T)$
6	$8.807 \cdot 10^{-4} \cdot \exp(-20{,}498.9/T)$	$1.035 \cdot 10^{-8} \cdot \exp(-7{,}156.7/T)$
8	$9.962 \cdot 10^{-4} \cdot \exp(-20{,}588.5/T)$	$6.182 \cdot 10^{-9} \cdot \exp(-6{,}506.1/T)$
10	$1.065 \cdot 10^{-3} \cdot \exp(-20{,}635.9/T)$	$4.632 \cdot 10^{-9} \cdot \exp(-6{,}141.5/T)$

Notably, the plot is divided into two sections and a different diffusion mechanism seems to occur in each section. The border between the sections is located at T = 1173 K. This temperature is close to the A_3-temperature of pure iron. Above the A_3-temperature the alloy is fully austenitized. We presume that the crystal structure of the ferrous substrate can strongly influence the kinetics of boriding and propose the following hypothesis.

Carbon, as an alloying element in steel, forms a solid solution in the Fe lattice, with carbon atoms occupying interstitial positions within it. Boron atoms have a similar atomic radius to carbon atoms, and thus, they may potentially occupy the same positions as carbon atoms in the lattice. In other words, boron diffuses competitively with carbon in the Fe substrates. Therefore, during boronization, while boron atoms diffuse into the lattice, carbon atoms are displaced away from the specimen surface, forced by the chemical potential gradient of boron. For this reason, we can assume that, at a small distance from the surface and before the formation of the boride layer, the material is structurally close to pure iron. Thus, the material becomes fully austenitized at approximately 1162 K.

Conversely, according to [27], the mobility of the carbon atoms in ferrite (BCC) is significantly increased compared to that in austenite (FCC). Therefore, in austenite, the above described displacement of carbon is obstructed, due to its low mobility in the FCC lattice. As a result, carbon atoms pile up, thereby creating a high carbon barrier in front of the coating/substrate interface. This barrier may also contain carbide grains, if the concentration of carbon locally exceeds the saturation limit. This carbon (or carbide) barrier acts as an obstacle for further boron diffusion towards the substrate, causing boronization to be less temperature-activated at these temperatures. Consequently, the slope of the ln$D$ versus 1/T diagram (**Fig. 8**) at T > 1173 K is decreased. In **Fig. 9**, the boride layer is presented.

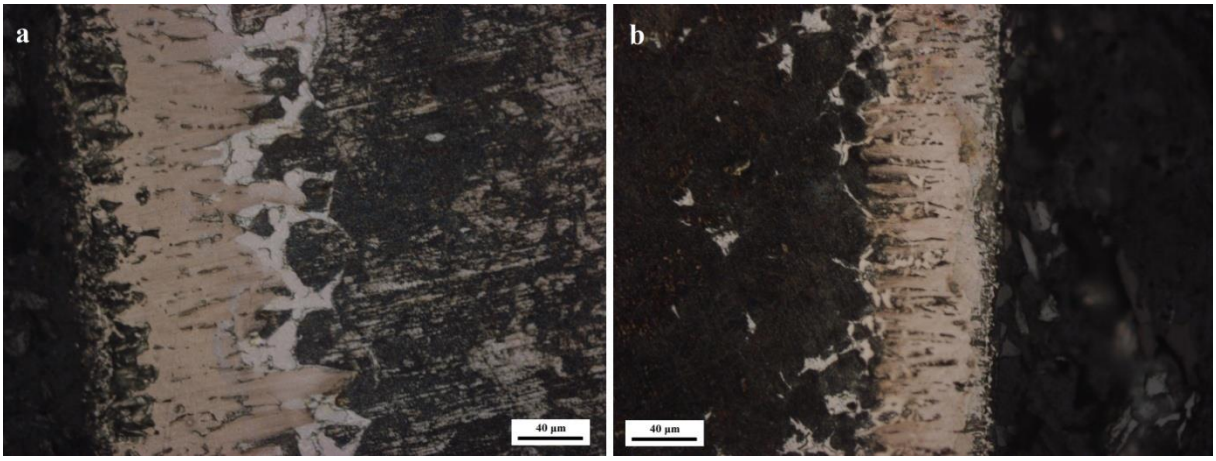


Fig. 9: Boride layer created (a) at 1273 K for 6 h and (b) at 1123 K for 10 h

From **Fig. 9a**, one can observe a wide high-carbon barrier (white area) in front of the coating with a dense carbide precipitations network. In **Fig. 9b,** this barrier is much thinner and less clear.

Additionally, a dependence of the diffusion coefficient on the boriding time can be observed, especially at low temperatures. In **Eq. 7**, a time variable appears in the γ-factor, which is eliminated as the temperature increases. For instance, at 1273 K, the incubation time t_0 is negligible; thus, no time-dependence of the diffusion coefficient is observed.

5. CONCLUSIONS

- A thick and hard tooth-like Fe_2B layer is formed during boriding treatment, which clearly passes the VDI 3198 test, especially at high boronizing temperatures.
- The boride layer displays a quite satisfactory hardness profile with the gradual decrease in the hardness perpendicular to the surface.
- The kinetic study revealed a clear and strong correlation of the diffusion coefficient with the crystal structure (i.e., FCC or mixed BCC/FCC) of the substrate during the process.
- A decrease in the coating thickness at long boronizing durations is observed, which was caused by reverse diffusion motion, due to time-dependent boron depletion phenomena.

ACKNOWLEDGMENTS

The authors acknowledge **Mrs. Dabou Xanthi** for carrying out the XRD measurements and **professor Pavlidou Eleni** for SEM analysis. This research has been financially supported by **General Secretariat for Research and Technology (GSRT)** and the **Hellenic Foundation for Research and Innovation (HFRI)** (Scholarship Code: 530).

REFERENCES

1. ASTM Steel 2016. 15 Common Applications for Versatile 4140 Steel, viewed 18 September 2018 <https://www.astmsteel.com/steel-knowledge/15-application-4140-steel/>.
2. Stewart, K 1997, 'Boronizing protects metals against wear', *Advanced Materials & Processes*, vol. 151, pp.23-25.
3. Von Matuschka, AG 1980, *Boronizing*, Germany: Carl Hansen Verlag.

4. Ataibis, V & Taktak, S, 2015, 'Characteristics and growth kinetics of plasma paste borided Cp–Ti and Ti6Al4V alloy', *Surface & Coatings Technology*, vol.279, pp.65-71.
5. Kayali, Y, 2015, 'Investigation of diffusion kinetics of borided AISI P20 steel in micro-wave furnace', *Vacuum*, vol. 121, pp.129-34.
6. Kulka, M, Makuch, N & Piasecki, A, 2017, 'Nanomechanical characterization and fracture toughness of FeB and Fe2B iron borides produced by gas boriding of Armco iron', *Surface & Coatings Technology*, vol. 325, pp.515-32.
7. Kulka, M, Makuch, N & Pertek, A, 2013, 'Microstructure and properties of laser-borided 41Cr4 steel', *Optics & Laser Technology*, vol.45, pp.308-18.
8. Dearnley, PA & Bell, T, 1985, 'Engineering the Surface with Boron Based Materials', *Surface Engineering*, vol. 1, pp.203-17.
9. Aichholz, SAdC, Meruvia, MS, Júnior, PCS & Ricardo Torres, D, 2018, 'Tribocorrosion behavior of boronized AISI 4140 steel', *Surface & Coatings Technology*, vol. 352, pp.265-72.
10. Campos-Silva, I et al., 2010, 'Characterization of AISI 4140 borided steels', *Applied Surface Science*, vol. 256, pp.2372-79.
11. Ulutan, M, Celik, ON, Gasan, H & Er, U, 2010, 'Effect of Different Surface Treatment Methods on the Friction and Wear Behavior of AISI 4140 Steel', *Journal of Materials Science & Technology*, vol. 26, pp.251-57.
12. Yılmaz, SO & Karatas, S, 2013, 'Effect of mechanical activation on jell boronizing treatment of the AISI 4140', *Applied Surface Science*, vol. 275, pp.148-55.
13. Sen, S, Sen, U & Bindal, C, 2005, 'The growth kinetics of borides formed on boronized AISI 4140 steel', *Vacuum*, vol. 77, pp.195-202.
14. Sen, S, Sen, U & Bindal, C, 2006, 'Tribological properties of oxidised boride coatings grown on AISI 4140 steel', *Materials Letters*, vol. 60, pp.3481-86.
15. Vidakis, N, Antoniadis, A & Bilalis, N, 2003, 'The VDI 3198 indentation test evaluation of a reliable qualitative control for layered compounds', *Journal of Materials Processing Technology*, vol. 143-4 pp.481-85.
16. Krelling, AP, da Costa, CE, Milan, JCG & Almeida, EAS, 2017, 'Micro-abrasive wear mechanisms of borided AISI 1020 steel', *Tribology International*, vol. 111, pp.234-42.
17. Ramdan, RD, Dadan, T & Tomita, Y, 2008, 'Free Energy Problem for the Simulations of the Growth of Fe_2B Phase Using Phase-Field Method', *Materials Transactions*, vol. 49, pp.2625-31.
18. Türkmen, I & Yalamaç, E, 2018, 'Growth of the Fe2B layer on SAE 1020 steel employed a boron source of H_3BO_3 during the powder-pack boriding method', *Journal of Alloys and Compounds*, vol. 2, pp.658-66.
19. Taktak, S, 2007, 'Some mechanical properties of borided AISI H13 and 304 steels', *Materials and Design*, vol. 28, pp.1836-43.
20. Kulka, M, Pertek, A & Makuch, N, 2011, 'The importance of carbon concentration–depth profile beneath iron borides for low-cycle fatigue strength', *Materials Science and Engineering A*, vol. 528, pp.8641-8650.
21. Pelleg, J, 2013, *Mechanical Properties of Materials*. New York: Springer.
22. Courtney, TH, 1999, *Mechanical Behavior of Materials*. 2nd ed. Boston, USA: McGraw-Hill.
23. Shetty, MN, 2013, 'Strenghtening by Putting Obstacles to Dislocation Motion', in Shetty, MN (ed.) *Dislocations and Mechanical Behaviour of Materials*. 1st ed. Delhi, India: PHI Learning Private Limited. Ch. 4.12.1. pp.415-19.

24. Dybkov, VI, 2016, 'Basics of Formation of Iron Boride Coatings', *Journal of Mineral Metal and Material Engineering*, vol. 2, pp.30-46.
25. Tomov, I, 1989, 'Effective Depth of X-Ray Penetration and Its Orientation Dependence', in J. Hasek, (ed.) *X-Ray and Neutron Structure Analysis in Materials Science*. Boston, MA, USA: Springer. pp.215-21.
26. *Adsorption Kinetics - The Rate of Adsorption*, viewed 18 September 2018, <http://www.chem.qmul.ac.uk/surfaces/scc/scat2_3.htm>.
27. Dahl, W, 1998, 'Band 1: Grundlagen', in Dahl, W (ed.), *Eigenschaften und Anwendungen von Stählen*. 5th ed. Aachen, Germany: Verlag-Mainz.